Smart Structures and Systems, *Vol. 17, No. 6 (2016) 1067-1085*
DOI: http://dx.doi.org/10.12989/sss.2016.17.6.1067

Stationary and nonstationary analysis on the wind characteristics of a tropical storm

Tianyou Tao, Hao Wang* and Aiqun Li

Key Laboratory of Concrete and Prestressed Concrete Structures of Ministry of Education, Southeast University, Nanjing 210096, China

(Received November 19, 2015, Revised April 4, 2016, Accepted April 9, 2016)

Abstract. Nonstationary features existing in tropical storms have been frequently captured in recent field measurements, and the applicability of the stationary theory to the analysis of wind characteristics needs to be discussed. In this study, a tropical storm called Nakri measured at Taizhou Bridge site based on structural health monitoring (SHM) system in 2014 is analyzed to give a comparison of the stationary and nonstationary characteristics. The stationarity of the wind records in the view of mean and variance is first evaluated with the run test method. Then the wind data are respectively analyzed with the traditional stationary model and the wavelet-based nonstationary model. The obtained wind characteristics such as the mean wind velocity, turbulence intensity, turbulence integral scale and power spectral density (PSD) are compared accordingly. Also, the stationary and nonstationary PSDs are fitted to present the turbulence energy distribution in frequency domain, among which a modulating function is included in the nonstationary PSD to revise the non-monotonicity. The modulated nonstationary PSD can be utilized to unconditionally simulate the turbulence presented by the nonstationary wind model. The results of this study recommend a transition from stationarity to nonstationarity in the analysis of wind characteristics, and further in the accurate prediction of wind-induced vibrations for engineering structures.

Keywords: tropical storm; wind characteristics; stationarity; nonstationarity; structural health monitoring

1. Introduction

In the past few decades, a great many remarkable cable-supported bridge projects have been constructed across the world. Most of them are famous for the main characteristics of long span length and apparent structural flexibility, e.g., the Akashi-Kaikyo Bridge in Japan with a main span of 1991 m, the Xihoumen Bridge in China with a main span of 1650 m and the Great Belt Bridge in Denmark with a main span of 1624 m. The cable-supported bridges are distinguished for the strong spanning capabilities due to inherent reasonable mechanical characteristics, and thus becoming one of the first choices to overcome rivers, seas and valleys (Gimsing 1983). However, long-span cable-supported bridges are so flexible structures that show obvious sensitivities to wind actions. This phenomenon is becoming increasingly evident with the increment of bridge span length. In recent years, the wind disasters are becoming more and more violent across the world, and result in the collapses of numerous engineering structures, which put forwards higher

*Corresponding author, Professor, E-mail: wanghao1980@seu.edu.cn

http://www.techno-press.org/?journal=sss&subpage=8 ISSN: 1738-1584 (Print), 1738-1991 (Online)

requirements to the wind-resistant performance of long-span cable-supported bridges. Hence for the long-span cable-supported bridges in wind-prone areas, especially for those bridges which are vulnerable to strong winds, improving the knowledge of the wind environment at the bridge site is crucial to the security of engineering structures. On the other hand, several modern and effective methods, including wind tunnel tests, computational fluid dynamics (CFD), finite-element-based numerical simulation, etc., have been successfully applied in the prediction of structural wind-induced responses (Cai *et al*. 1999, Chen and Kareem 2002, Zhu and Xu 2005, Chen *et al*. 2009, Wu and Kareem 2015). However, the accuracy of predicted results heavily depends on the precise assessment of the site wind characteristics. As a result, it is necessary to conduct field measurements on the wind characteristics at the bridge site to guide or verify the existing analytical theories (Xu *et al*. 2000, Wang *et al*. 2013).

The characteristics of strong winds in the atmospheric boundary layer have always been a hot research subject in structural wind engineering (Ishizaki 1983, Li *et al*. 2009). At present, two main weather systems are usually concentrated on in the study of strong winds. One is the monsoon climate due to sea-land thermal differences; the other refers to the tropical cyclones mostly derived on the Pacific Ocean (Meng *et al.* 1997). A great deal of work about monsoon characteristics has been carried out in the early stage. Due to the structural characteristics of tropical cyclones and their huge destructive powers, the current study of wind characteristics mainly focuses on the latter. Actually, natural wind is inherently turbulent, which means the wind velocity and wind direction are random in a short time. Hence, it is essential to extract reliable statistical information, which can represent the faithfulness of local wind regime, from massive real-time measured data, so that the requirements for the design and construction of engineering structures can be satisfied. This actually depends on the wind data collection in field measurements and long-term monitoring of the wind characteristics at the bridge site (Wang *et al.* 2013). Some pioneering research work on the characteristics of tropical cyclones have been conducted based on field measurements, and some useful empirical models about wind characteristics are proposed (Von Karman 1948, Bush and Panofsky 1968, Kaimal 1972, Choi 1978, Kareem 1985). These fruitful results have been adopted by some national specifications and widely utilized in the wind-resistant design and analysis of engineering structures.

The aforementioned researches mainly focus on the stationary characteristics of strong wind fields, in which the wind velocity is treated as a stationary random process with a constant mean. However, some existing field measurement results have indicated that the wind velocity often exhibits unstable mean and variance during a tropical cyclone, which means the measured wind velocity is nonstationary (Xu and Chen 2004, Wang and Kareem 2004, Wu 2015). In this situation, it is difficult to accurately estimate the wind characteristics of a tropical cyclone due to the unavailability of stationary hypothesis. In order to better understand the wind characteristics of a tropical cyclone as well as its effects on engineering structures, new analytical methods need to be adopted for the analysis of measured wind records and statistically extract valuable information in a nonstationary condition. At present, some antecedent researches on the nonstationary wind characteristics have been conducted. For example, Xu and Chen (2004) proposed a nonstationary model of wind velocities in view of the features of measured wind records and did a careful comparison with the traditional wind velocity model. Based on empirical mode decomposition and wavelet transform, Wang and Kareem (2004) successfully extracted the time-varying mean of a hurricane and conducted a discussion on related wind characteristics. With the aid of wavelet transform, McCullough and Kareem (2013) extended the traditional surrogate method to time-frequency domain so that the nonstationary features of wind records can be well examined.

The existing researches on the nonstationary wind characteristics of tropical cyclones are at an early stage, more field measurements are still needed during long-term monitoring so that the wind data can be accumulated, offering the potential to perfect existing nonstationary wind velocity model and gradually establish a nonstationary database.

In this paper, the tropical storm, which is named as Nakri, is taken as the research object. The wind records were fully recorded at Taizhou Bridge site by the anemometer in the SHM system. The stationarity of the wind velocity is evaluated with the nonparametric run test method. And then, a comparative study on the wind characteristics, e.g., mean wind velocity, turbulence intensity, turbulence integral scale, turbulence power spectral density, etc., is conducted based on stationary and nonstationary wind velocity models. Several results are derived during the analytical procedure and conclusions are given in the end.

2. Data source and typhoon descriptions

2.1 Introduction to Taizhou Bridge

Taizhou Bridge, which is short for Taizhou Yangtze River Bridge, is located in the lower reach of the Yangtze River in China, and first establishes the connection of land transportation between Taizhou and Zhenjiang, as shown in Fig. 1. Since it was open to traffic in 2012, it has been the first longest triple-tower suspension bridge in the world with a continuous main span of 2×1080 m. In respect to the geographical location, Taizhou Bridge is located in the eastern part of the Asian continent, which belongs to a wind-prone area that is vulnerable to the typhoons from the west Pacific Ocean in summer. As long-span bridges are sensitive to the wind actions due to the inherent flexible features, the wind environment at the Taizhou Bridge site should be specifically monitored to accurately evaluate the wind characteristics.

2.2 Layout of the anemometer

The development of SHM technology has provided an efficient approach to monitor the environmental actions on engineering structures (Ou and Li 2010, Ni *et al*. 2012, Ye *et al*. 2013). In order to monitor the wind environment at Taizhou Bridge site, a WA15-type anemometer is included in the SHM system. As shown in Fig. 2, this anemometer is installed on top of the middle tower with 194 m above the ground. The WA15 anemometer, made by Vaisala Company in Finland, is a high-performance device used for the measurement of wind velocity and direction. Numerous applications in meteorology have proved the efficiency and accuracy of this kind anemometer in wind measurements. The wind velocity ranging from 0.4 m/s to 75 m/s can be accurately recorded with a resolution of 0.1m/s, while the measurement range of wind direction is between 0° and 359° with a resolution of 1°. The anemometer can steadily work in a temperature environment from -5℃ to +55℃. During the long-term monitoring, the sampling frequency of the anemometer is set as 1 Hz. The azimuth angle 0° is defined as due north, positively rotating in a clockwise direction. More than two years' usage has indicated that the anemometer works in a stable condition. Several wind records of strong winds, including both typhoon and monsoon winds, have been successfully recorded and the reliability has been verified by some additional field measurements.

Fig. 1 Geographical location of Taizhou Bridge

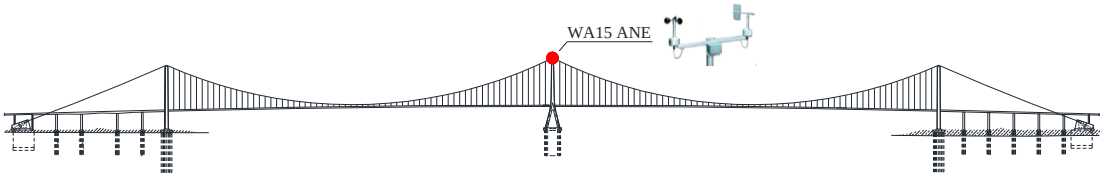

Fig. 2 Installation of the anemometer on Taizhou Bridge

2.3 Description of the tropical storm Nakri

Nakri is the 12th strong tropical storm in 2014. It was born as a tropical depression on the ocean surface in the southeastern part of Taiwan on July 17. On July 30, it was developed into a tropical storm and presented obvious monsoon depression features. The wind pressure in the outer region is much stronger than that in the central area, and a rare huge convective hollow was even captured in the central part. At that time, the wind velocity near surface had achieved 18 m/s. Then, Nakri moved towards north with a speed of 20km/h and entered the East China Sea. On August 1, it was further evolved into a strong tropical storm and the maximum wind velocity near surface has achieved 25 m/s. After leaving the East China Sea, Nakri degraded to a tropical storm and then moved towards northeast to enter the Yellow Sea. On August 3, the intensity of Nakri decreased to a level of a tropical depression and disappeared in the next day. The whole moving routine of Nakri is in detail shown in Fig. 3.

2.4 Measured wind data

Taizhou Bridge was within the moderate gale region of the strong tropical storm Nakri. The anemometer on top of the middle tower successfully recorded the wind velocity and direction in

real time when Nakri passed by the bridge site. 16 hours of the wind records when the storm is nearest to the bridge site is taken as the research object, as shown in Fig. 4. The wind direction is recorded in the range from 0° to 359°, so it will present a spurious oscillation in the figure when the wind direction changes from 359° to 0°. In order to continually and intuitively describe the changes of the wind direction, the azimuth angle over 180° is shown Fig. 4 in a negative form. The real wind direction should be the summation of the negative value and 360°. As shown in Fig. 4, the measured wind velocity apparently presents obvious time-varying features, while the measured direction is relatively stable except for some periods.

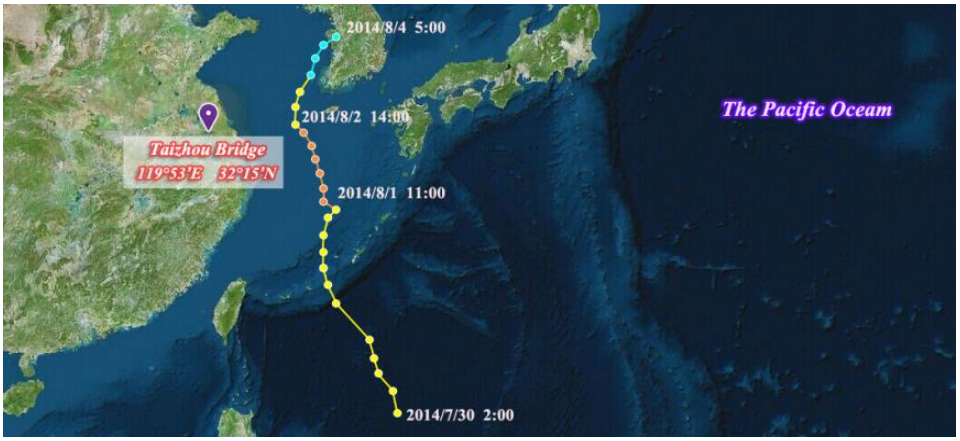

Fig. 3 Moving routine of the tropical storm "Nakri"

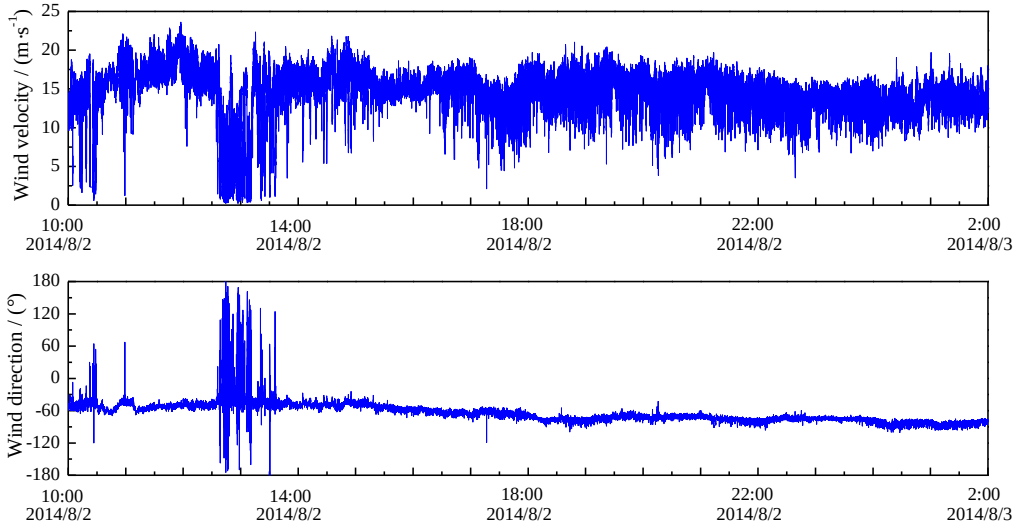

Fig. 4 Measured wind velocity and direction of Nakri at the bridge site

3. Stationary evaluation of measured wind velocity

In traditional analysis of strong winds, the premise that the statistical parameters have the physical meanings is that the wind velocity in a given time interval can satisfy with the stationary hypothesis (Cao *et al.* 2015). However, due to the inherent features built in tropical storms, the measured wind velocity usually shows obvious time-varying tendencies, indicating the wind velocity is nonstationary. In such cases, the stationarity of the wind samples must be in advance evaluated by studies of available wind records before analyzing the wind characteristics of Nakri.

Nowadays, several methods are available to evaluate the stationarity of data series, e.g., the run test method and the reverse arrangement method (McCullough and Kareem, 2013). In this paper, the run test method is adopted to conduct stationary evaluation for the wind velocity of Nakri. The run test method detects the existence of underlying trends of a signal in the view of hypothesis testing. In the testing procedure, no knowledge of the probability distribution of the data being evaluated is required. Hence, it is naturally a distribution-free or nonparametric procedure and suitable for the stationary evaluation of data series with arbitrary probability distributions.

The principle of the run test is as follows. Consider a sequence of N observed values of a random variable x_i (i=1, 2, 3, ..., M) with a mean value of $\bar{x}$ where each observation is classified into one of two mutually exclusive categories, which can be identified simply by plus (+) when $x_i>\bar{x}$ or minus (-) when $x_i<\bar{x}$. The sequence of plus and minus observations can be obtained, as shown in Fig. 5, which is an example of the run test on measured wind samples. A run is defined as a sequence of identical observations that is followed by a different observation or no observation at all. In application, the random variable is usually selected as either the mean value or the variance of wind samples, thus the nonstationarity characterized by time-varying mean or time-varying variance can be well evaluated. In present study, each sample of 1 hour duration is divided into 60 segments to count the number of runs. When the number of segments is sufficient, the number of runs R will obey an approximate Gaussian distribution and the probability density function can be expressed as N(μ, σ^2), where μ and σ can be calculated in terms of Eq. (1). In Eq. (1), m is the number of plus in a whole observation while n is the number of minus.

Let it be hypothesized that the sample tested is a stationary random process, so that the hypothesis can be accepted or rejected according to the number of runs. If there are too many runs, the length of each run will be short, indicating that the plus and minus will appear periodically. If the runs are too few, the plus or minus will appear in groups. On this circumstance, too many and too few runs both indicate an underlying trend exists in the tested data series, which means the sample is nonstationary. In the view of hypothesis testing, the acceptance region for the aforementioned hypothesis is $\varphi_{1-\alpha/2} < \varphi < \varphi_{\alpha/2}$, where $\varphi_{1-\alpha/2}$ and $\varphi_{\alpha/2}$ are the percentage point that satisfy Prob[$\varphi < \varphi_{1-\alpha/2}$]= $\alpha/2$, Prob[$\varphi > \varphi_{\alpha/2}$]= $\alpha/2$, and α is the desired level of significance in a two-sided test (Bendat and Piersol 2010).

In present study, the desired level of significance is taken as 5%, so the acceptance region naturally can be expressed as (μ-1.96σ, μ+1.96σ). If the number of runs R falls in the acceptance region, the hypothesis will be accepted which means there is no evidence of an underlying trend existing in the tested data series. In the example shown in Fig. 5, the acceptance regions for the two cases are (22.25, 36.48) and (23.08, 37.86), respectively. The wind velocity in Fig. 5(a) is judged as stationary because the number of runs (R=33) falls within the range between 22.25 and 36.48, while the one in Fig. 5(b) is nonstationary because the number of runs (R=15) is smaller than the lower boundary of the acceptance region.

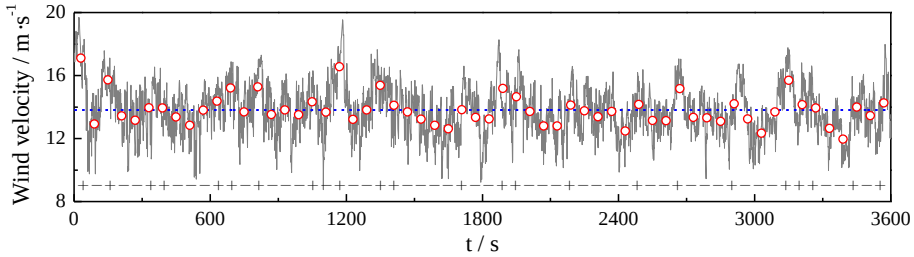

(a) stationary data (R=33)

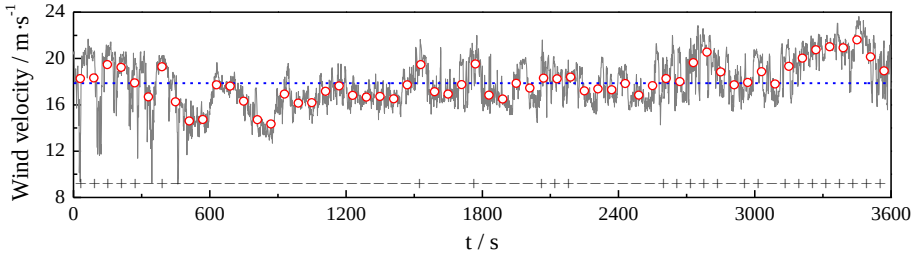

(b) nonstationary data (R=15)

Fig. 5 Examples of the run test on measured wind samples

$$\mu = \frac{2mn}{m+n} + 1 \tag{1a}$$

$$\sigma = \sqrt{\frac{2mn(2mn-m-n)}{(m+n)^2(m+n-1)}} \tag{1b}$$

In the traditional stationary model, the 2D wind velocity is regarded as a vector that can be decomposed into along-wind velocity and cross-wind velocity according to the main wind direction (Simiu and Scanlan, 1978). The along-wind and cross-wind velocity can be described as Eq. (2). In Eq. (2), $U(t)$ is the along-wind velocity; $V(t)$ is the cross-wind velocity; $\bar{U}$ is the constant mean wind velocity; $u(t)$ and $v(t)$ are along-wind and cross-wind zero-mean fluctuating wind velocities, respectively.

$$U(t) = \bar{U} + u(t) \tag{2a}$$

$$V(t) = v(t) \tag{2b}$$

Based on the aforementioned stationary model, the run test method is utilized to evaluate the stationarity of along-wind and cross-wind velocities of Nakri. The tested cases include both the mean value and the variance. With a time interval of 1h, the measured wind record is divided into 16 samples and the stationary evaluation results are presented in Table 1. As shown in Table 1, the mean value performs prominent nonstationary tendencies in both along-wind and cross-wind cases, while the nonstationarity in variance is comparatively weak. For the mean value, 87.5% of the segments cannot pass the stationary test in along-wind case while the proportion for cross-wind

case is 93.75%. For the variance, only 37.5% of the segments cannot pass the stationary test in along-wind case while the percentage for cross-wind case is more than 50%, indicating a stronger nonstationarity existing in the variance of cross-wind velocity than that of along-wind case. Taken together, the wind velocity of Nakri shows distinct nonstationary features, especially for the mean value proved to be with prominent time-varying trends, which is contradictory to the traditional stationary assumptions. Therefore, a nonstationary wind model is included in the following parts to conduct a further analysis on the wind characteristics of Nakri.

4. Mean wind characteristics

For the parameters concerning wind characteristics, some nonstationary models have been proposed by many talented scholars based on the traditional stationary model (Chen and Xu 2004, Wang and Kareem 2004, Chen *et al.* 2007). There are some minor differences in the parameter definitions of wind characteristics, but their knowledge to the nonstationary model is the same, as expressed by Eq. (3). In the nonstationary wind model, both along-wind and cross-wind velocities are treated as the summation of a time-dependent trend called time-varying mean and the residual turbulence, which means the wind velocity is decomposed into a low-frequency part and a high-frequency part.

$$U(t) = \bar{U}^*(t) + u^*(t) \tag{3a}$$

$$V(t) = \bar{V}^*(t) + v^*(t) \tag{3b}$$

where $U(t)$ is the along-wind velocity; $V(t)$ is the cross-wind velocity; $\bar{U}^*(t)$ is the time-varying wind velocity in along-wind direction; $\bar{V}^*(t)$ is the time-varying wind velocity in cross-wind direction; $u^*(t)$ is the along-wind fluctuating wind velocity called along-wind nonstationary turbulence in the following parts; $v^*(t)$ is the cross-wind fluctuating wind velocity called cross-wind nonstationary turbulence in the following parts. Obviously, if the measured wind velocity is a stationary process, the time-varying wind velocities in Eq. (3) will degenerate into constant means so that Eq. (3) will be unified with Eq. (2).

One of the key issues in the application of nonstationary wind model is to approximately extract the time-varying mean from a given wind sample (Chen and Xu 2004, Wang and Kareem 2004, Chen and Letchford 2004). Currently, two efficient methods, including empirical mode decomposition and multi-level wavelet transform, are available for the extraction of the underlying trends existing in wind records. Due to the strict dyadic decomposition and definite physical meaning, wavelet-based method is utilized to peel off the time-varying mean from along-wind and cross-wind samples in this study. Among the procedure, the 10^{th}-order Daubechies wavelet is taken as the mother wavelet and each record is decomposed into 7~9 levels according to the decomposed effects. The residual low-frequency level is treated as the time-varying trend of the analyzed wind record. Taking the fifth sample of the wind records as an example, the mean wind velocities based on stationary and nonstationary models are shown in Fig. 6, which is accompanied by the original records. It is easy to find that the time-varying mean well satisfies with the variation trend of the original record, and thus is more suitable for the description of the mean wind velocity of nonstationary wind record than the constant mean.

Table 1 Stationary evaluation of the measured wind samples

Cases	Along-wind		Cross-wind	
	Mean value	Variance	Mean value	Variance
Nonstationary portion	87.50%	37.50%	93.75%	56.25%
Stationary portion	12.50%	62.50%	6.25%	43.75%

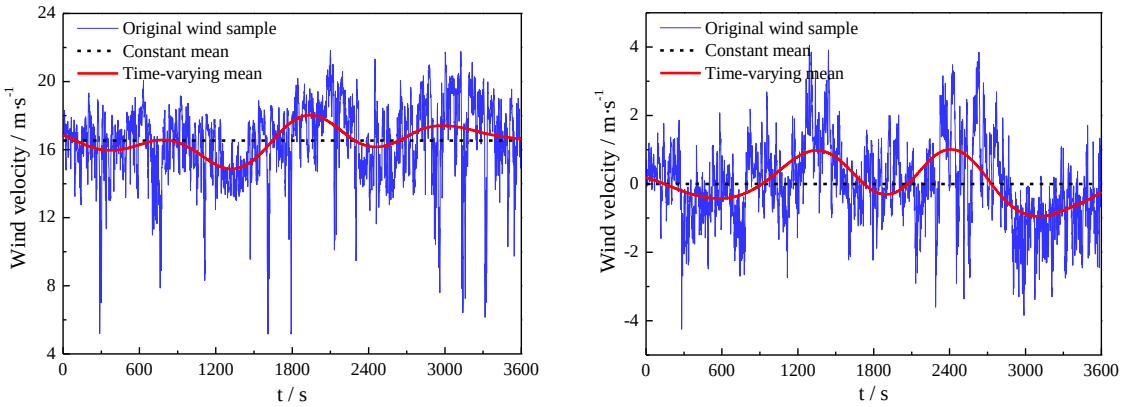

(a) along-wind velocity (b) cross-wind velocity

Fig. 6 Comparison of mean wind velocities from stationary and nonstationary models

After removing the time-varying trends, a run test is also conducted on the nonstationary turbulence for both along-wind and cross-wind cases. The analytical results are shown in Table 2. Compared with Table 1, the nonstationary proportion of along-wind turbulence about mean value dropped from 87.5% to 31.25%, while that of cross-wind turbulence decreases from 93.75% to 31.25%. This phenomenon indicates that the stationarity of $u^*(t)$ and $v^*(t)$ is rapidly increased with the extraction of time-varying trends, and they can be treated as stationary processes in the nonstationary wind model, which verifies the stationary hypothesis by Xu *et al*. (2004) and Wang *et al.* (2004). However for the variance, the along-wind nonstationary proportion increases from 37.5% to 50.0% while the cross-wind nonstationary proportion decreases from 56.25% to 31.25%, indicating that the influence of extracting the time-varying mean on the stationarity of variance is not exclusive. That means the nonstationary wind model on the aspect of variance stationarity still needs to be improved.

Table 2 Stationary evaluation of the residual fluctuating wind samples

Cases	Along-wind		Cross-wind	
	Mean value	Variance	Mean value	Variance
Nonstationary portion	31.25%	50.00%	31.25%	31.25%
Stationary portion	68.75%	50.00%	68.75%	68.75%

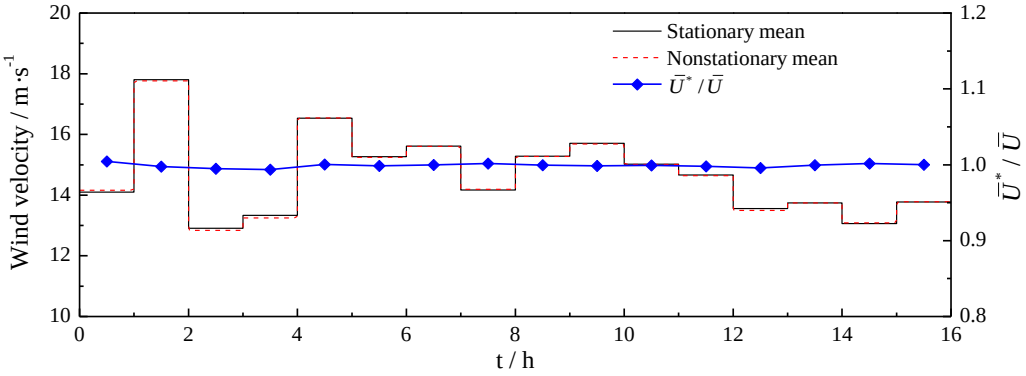

Fig. 7 Comparison of stationary and nonstationary mean wind velocity

In order to compare stationary and nonstationary wind characteristics in a same physical meaning, a nonstationary average wind velocity is defined as the mean value of along-wind time-varying wind velocity over the whole time duration, as expressed in Eq. (4).

$$\bar{U}^* = \frac{1}{T}\int_0^T \bar{U}^*(t)dt \tag{4}$$

Stationary and nonstationary average wind velocities of the given wind records are calculated, and a comparison of $\bar{U}^*$ and $\bar{U}$ is shown in Fig. 7. In each segment, the stationary average wind velocity $\bar{U}$ is almost the same as the nonstationary average wind velocity $\bar{U}^*$, apparently manifesting the ratio $\bar{U}^*/\bar{U}$ approaches one through the time. This phenomenon indicates that the time-varying mean fluctuates around the constant mean and they are unified in terms of the mean value. In such a case, the nonstationary wind model can be easily applied in engineering practices since the traditional average wind velocity can still be used in the nonstationary model. For the cross-wind time-varying mean, the corresponding mean value in each time interval is close to zero, which shows the same discipline as along-wind cases.

5. Turbulent wind characteristics

5.1 Turbulence intensity

Turbulence intensity is a key parameter that represents the ratio of turbulence in natural wind. In the traditional wind model, it is defined as the ratio of the standard deviation of turbulence and the mean wind velocity in a given time interval, as expressed in Eq. (5(a)). In order to make the turbulence intensity in nonstationary wind model have the same physical meaning as that of the stationary model, the nonstationary turbulence intensity is defined as Eq. (5(b)).

$$I_u = \frac{\sigma_u}{\bar{U}} \qquad I_v = \frac{\sigma_v}{\bar{U}} \tag{5a}$$

$$I_u^* = \frac{\sigma_u^*}{\bar{U}^*} \qquad I_v^* = \frac{\sigma_v^*}{\bar{U}^*} \tag{5b}$$

where I_u and I_v are along-wind and cross-wind turbulence intensities in the stationary wind model, respectively; σ_u and σ_v are the standard deviations of along-wind and cross-wind stationary turbulence, respectively; I_u^* and I_v^* are along-wind and cross-wind turbulence intensities in the nonstationary wind model, respectively; σ_u^* and σ_v^* are the standard deviations of nonstationary turbulences in along-wind and cross-wind cases, respectively.

Based on the two models in Eq. (5), the turbulence intensities of Nakri are calculated, as shown in Fig. 8. It is easy to find that the stationary turbulence intensity is totally larger than nonstationary turbulence intensity in both along-wind and cross-wind directions. This is mainly attributed to the stripping of the underlying trend existing in original wind records. The removing of the time-varying trend takes away the additional fluctuating wind velocity which results from the time-dependent variation of the mean wind velocity. In an apparent view, the differences of stationary and nonstationary turbulence intensities in the cross-wind direction are quite stable. However for the along-wind direction, the nonstationary turbulence intensity is much smaller than the stationary case from 3rd to 4th hour. The main reason of this phenomenon is that the rapid variation of wind velocity and direction in Fig. 4 during this period prominently improves the nonstationarity of along-wind wind samples.

In order to quantify the difference between stationary and nonstationary turbulence intensities, a ratio between nonstationary and stationary turbulence intensities, named as TI ratio in the following parts, is calculated in both along-wind and cross-wind directions, as listed in Table 3. The TI ratio of along-wind cases changes in the range [0.5412, 0.9733], while that of cross-wind cases ranges from 0.6152 to 0.8597. The upper limit means that the turbulence intensities based on stationary and nonstationary models differs not too much from each other for the stable wind samples which can satisfy with stationary assumption. On the contrary, the lower limit stands for an overestimation of the turbulence intensity by the stationary model for nonstationary wind records, thus indicating the nonstationary wind model will be much more reasonable. Just for the 16 hours wind records of Nakri, the mean value of TI ratio is 0.8777 in along-wind direction and 0.7892 in cross-wind direction, which means a 12.23% overestimation for along-wind turbulence intensity and a 21.08% overestimation for cross-wind direction by the traditional wind model. In addition, the mean ratio I_v/I_u is 0.4320 when stationary model is adopted and 0.4061 by nonstationary model. These two values deviate little from each other, so it can be concluded that the ratio of cross-wind and along-wind turbulence in nonstationary case is almost consistent with that in stationary case. Since 10min is usually taken as the time interval in some countries, the turbulence intensities in this study are not compared with the recommended values in codes.

Table 3 Comparison of stationary and nonstationary turbulence intensity cases

Cases	TI ratio			Stationary	Nonstationary
	max	min	average	I_v/I_u	I_v^*/I_u^*
Along-wind	0.9733	0.5412	0.8777	0.4320	0.4061
Across-wind	0.8597	0.6152	0.7892		

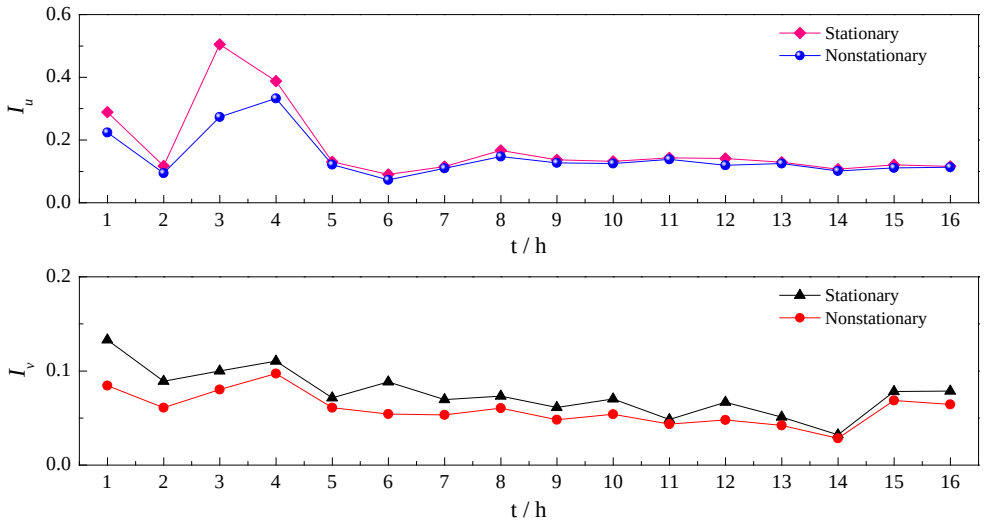

Fig. 8 Comparison of turbulence intensities based on stationary and nonstationary models

5.2 Turbulence integral scale

Turbulence integral scale is the measure of the average size of turbulent eddies in the flow. In the traditional stationary model, turbulence integral scale is mathematically defined as Eq. (6(a)) based on Taylor hypothesis. Keeping the physical meaning unchanged, the nonstationary model of turbulence integral scale is naturally presented as Eq. (6(b)) with corresponding nonstationary parameters instead of stationary parameters.

$$L_i = \frac{\bar{U}}{\sigma_i^2}\int_0^\infty R_i(\tau)d\tau \quad i = u, v \tag{6a}$$

$$L_i^* = \frac{\bar{U}^*}{\sigma_i^{*2}}\int_0^\infty R_i^*(\tau)d\tau \quad i = u, v \tag{6b}$$

where L_i and L_i^* are stationary and nonstationary turbulence integral scales, respectively; R_i and R_i^* are auto-covariance functions of the stationary and nonstationary fluctuations, respectively; τ is the time. It should be noted that the upper limit of integral is suggested to take the first t where $R_i(t)=0.05\sigma_i^2$ in case of large errors caused by Taylor hypothesis when the auto-covariance is small (Flay and Stevenson 1998).

Based on the two models, the stationary and nonstationary turbulence integral scales of Nakri are calculated, as shown in Fig. 9. The along-wind and cross-wind turbulence integral scales obtained by nonstationary model are much smaller than those from stationary model. It has been long recognized that the estimates of turbulence scales depend significantly upon the length and the degree of stationarity of the wind record being analyzed (Simiu and Scanlan 1996). That means the nonstationarity existing in the wind samples will cause the overestimation of turbulence

integral scales. In addition, the ratio between cross-wind and along-wind turbulence integral scale is suggested to be 0.33 based on long-term measurements (Counihan 1975). The values in this study are 0.70 for stationary model and 0.22 for nonstationary model, respectively. Obviously, the value from a nonstationary model is much more close to the suggested value, because the fluctuating wind can be treated as a stationary process after removing the time-varying trend. In this respect, the nonstationary wind speed model is more appropriate for the estimation of turbulence integral scale than the traditional stationary model. Furthermore, the turbulence integral scale is related to the position of the peak frequency in a spectrum (e.g., Karman spectrum) as a role of the Monin coordinate, so the estimation of turbulence integral scales may influence the dynamic responses of wind-sensitive structures, which is deserved for further studies.

5.3 Turbulence power spectral density

For the stationary and nonstationary spectral analysis, a 2h segment of the along-wind records (UTC+8, 15:00-17:00, 2014/8/2) is taken as an example. The original time history is fully shown in Fig. 10. Meanwhile, the constant mean in stationary model accompanied by time-varying mean in nonstationary model is plotted for comparisons.

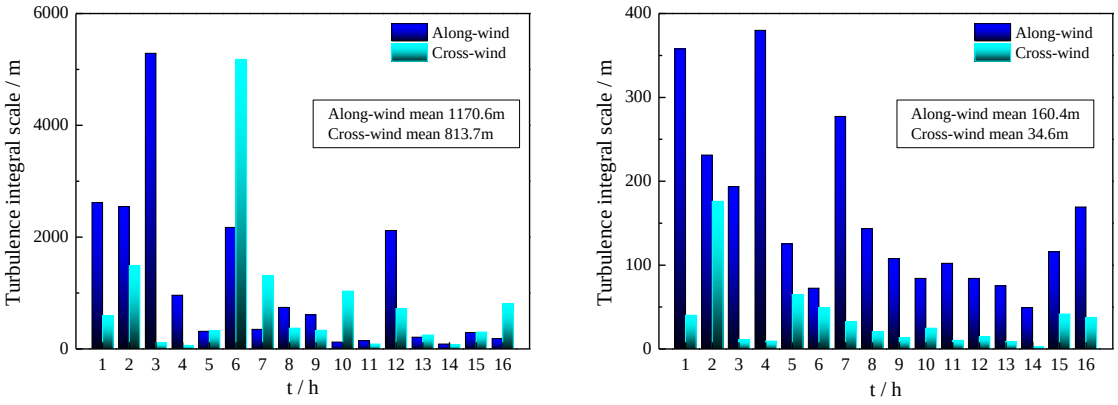

(a) Stationary (b) Nonstationary

Fig. 9 Stationary and nonstationary turbulence integral scales of measured samples

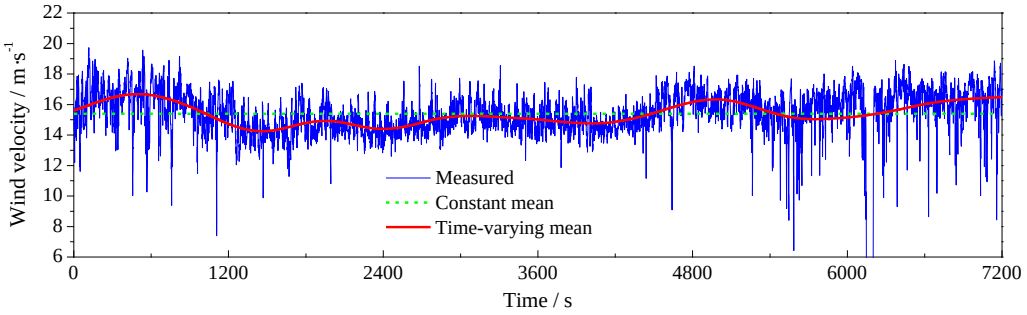

Fig. 10 Wind records for turbulence power spectral density analysis

After removing the constant mean and the time-varying mean, the stationary and nonstationary turbulences are derived accordingly. Based on the Welch transform, the PSD which presents the energy distribution of turbulence can be acquired from fluctuating wind velocities. Hence, the stationary and nonstationary PSDs are obtained with the aid of this procedure, as shown in Fig. 11. As indicated in Fig. 11, the nonstationary PSD is obviously lower than the stationary PSD in low-frequency ranges while they are almost the same in other regions. This is attributed to the extraction of time-varying mean which is physically appeared in terms of a low-frequency signal. For long-span bridges dominated by low-frequency mode shapes, the energy fading in the low-frequency ranges may greatly influence the prediction of structural wind-resistant performances. And thus special attention should be given to the low-frequency regions of the nonstationary PSD.

Since a number of spectral descriptions have been advanced primarily in strong tropical winds, the commonly used Simiu spectrum (Simiu and Scanlan 1996) and Karman spectrum (Von Karman 1948) in specifications are employed for comparison in this study. These spectra including both stationary and extended nonstationary cases are as below.

Karman spectrum:

$$\frac{nS(n)}{(u^*)^2} = \frac{4\beta f}{(1+70.8f^2)^{5/6}} \tag{7}$$

where n is the natural frequency of wind; $S(n)$ is the power spectral density of along-wind turbulence; u^* is the friction wind velocity; β is the coefficient of friction wind velocity. β and u^* have a relationship that can be described as $\sigma^2=\beta(u^*)^2$. σ is the standard deviation of stationary or nonstationary turbulence; $f = nL_u / U$ is the Monin coordinate; L_u is the turbulence integral scale, which can be taken as L_u in stationary model and L_u^* in nonstationary model; U is the mean wind velocity over the analyzed duration, which is $\bar{U}$ for stationary model and $\bar{U}^*$ for nonstationary model.

Simiu Spectrum

$$\frac{nS(n)}{(u^*)^2} = \frac{200f^*}{(1+50f^*)^{5/3}} \tag{8}$$

where $f^* = nZ / U$ is the Monin coordinate; Z is the altitude of the wind velocity; the friction wind velocity u^* is verified to be related to the standard deviation of turbulence σ, which can be presented as

$$\sigma^2 = 6(u^*)^2 \tag{9}$$

The remaining parameters in Eq. (8) are the same as those of Eq. (7). It should be noted that Eq. (8) and Eq. (9) will be stationary spectrum if the parameters from stationary wind model are employed, otherwise those will be extended nonstationary spectral models for turbulence.

During the comparison of measured PSDs and recommended spectral models, the stationary Simiu spectrum, nonstationary Simiu spectrum and stationary Karman spectrum all cannot well describe the measured spectrum, mainly presenting the features that higher in low-frequency bands and lower in high-frequency bands than measured PSDs. However for the nonstationary Karman spectrum, it can fit well with the measured PSDs in the inertial subrange (high-frequency region), and falls somewhere between measured stationary and nonstationary spectra in low-frequency region. The difference between stationary and nonstationary Karman spectra indicates that the selection of turbulence integral scale is vital to the specific expression of the spectral model, which verifies the aforementioned conclusion. Above all, both Simiu spectrum and Karman spectrum are difficult to perfectly describe the measured spectra for both stationary and nonstationary cases. In order to accurately predict the buffeting performance of engineering structures in this region, an empirical model, which can truly present the turbulent energy distribution, is still needed through nonlinear fitting.

Hence taking Eq. (10) as the benchmark, both the stationary and nonstationary measured spectra are fitted with the nonlinear square method. The specific empirical spectral models are explicitly expressed in Eq. (11). For a direct comparison, the fitted spectrum versus measured spectrum is plotted in Fig. 12.

$$\frac{nS(n)}{(u^*)^2} = \frac{Af^*}{(B + Cf^{*\alpha})^{\beta}} \tag{10}$$

where A, B, C, α, β are undetermined parameters for fitness. According to the Kolmogrov hypothesis, α and β should satisfy with an equation that $\alpha\beta$=5/3.

Stationary
$$\frac{nS(n)}{(u^*)^2} = \frac{807.56 f^*}{(1.92 + 7.12 f^{*0.52})^{5/1.56}} \tag{11a}$$

Nonstationary
$$\frac{nS(n)}{(u^*)^2} = \frac{214.43 f^*}{(5.91 + 19.56 f^{*0.99})^{5/2.97}} \tag{11b}$$

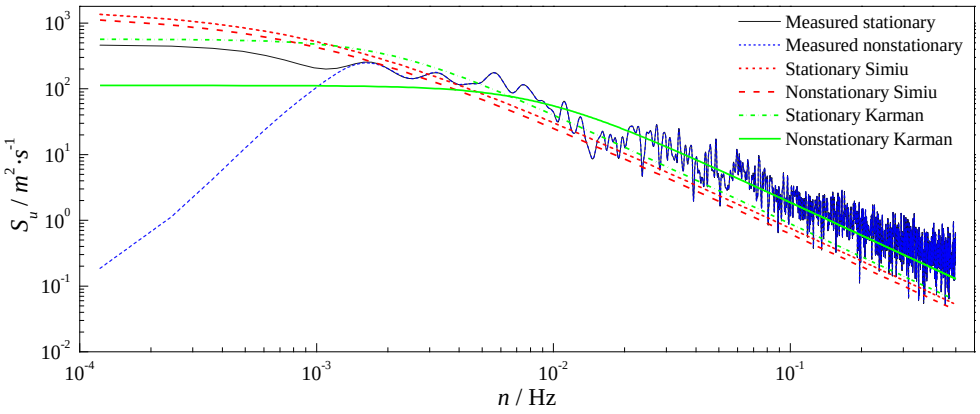

Fig. 11 Comparison of the measured PSD and recommended spectral models

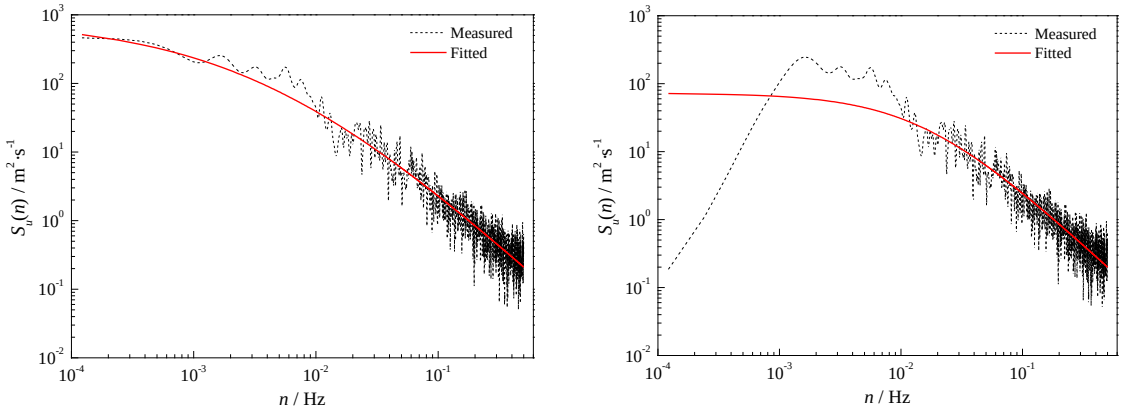

(a) Stationary (b) Nonstationary

Fig. 12 Parameter fitting of measured stationary and nonstationary PSDs

As shown in Fig. 12, the fitted spectrum is well satisfied with the measured stationary spectrum, indicating that the turbulence energy distribution of Nakri can be truly described by the fitted spectrum. However for the nonstationary spectrum, the measured spectrum can only satisfy with the fitted spectrum in the initial subrange. Due to the monotonicity of the benchmark model, the fitted spectrum cannot be identical to the non-monotonic features in the low-frequency range. Hence, the nonstationary fitted spectrum needs to be further modified according to the measured nonstationary spectrum.

A modulating function is included to revise the non-monotonicity of the benchmark model, so that the difference between measured and fitted spectra in the nonstationary case can be circumvented. With the modulating function, the nonstationary empirical spectral model can be expressed as

$$S^*(n) = S(n) \times A(n) \tag{12}$$

where $S(n)$ is the fitted spectrum in Eq. (11b); $S^*(n)$ is the modified spectrum; $A(n)$ is the modulating function concerned about the natural frequency of turbulence. The modulating function can be fitted according to the ratio between measured spectrum and fitted spectrum in a logarithmic coordinate. And the modulating function in this paper is detailed as

$$A(n)=\begin{cases} \exp(2.7929\ln n+19.2145) & 0\leqslant n\leqslant 0.0017 \\ \exp(-0.56376\ln n-2.1915) & 0.0017<n\leqslant 0.0205 \\ 1 & n>0.0205 \end{cases} \tag{13}$$

After a modulated modification, the final nonstationary empirical spectral model is obtained, as shown in Fig. 13. It can be seen that the modified spectrum can perfectly satisfy with the nonstationary measured spectrum, indicating that a hybrid procedure combining the nonlinear fitting and modulating revision can efficiently present a mathematical model that well describe the nonstationary PSD.

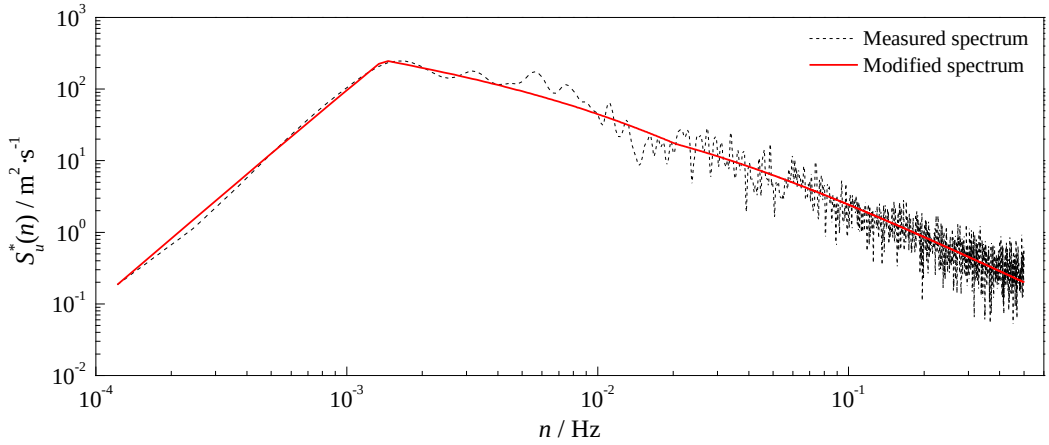

Fig. 13 Comparison of the measured nonstationary PSD and the modified spectrum

6. Conclusions

In this paper, the stationary and nonstationary analysis on the wind characteristics of a tropical storm is conducted based on SHM. A careful study on both the mean and turbulence wind characteristics is performed. The following conclusions can be drawn accordingly.

(1) After removing the time-varying trend, the mean-value nonstationarity of the fluctuating wind sharply decreases so that the turbulence in nonstationary wind model can be treated as a stationary process. However, the influence of this extraction is not consistent in the variance of the fluctuating wind, indicating that some improvements are needed in the variance stationarity for the nonstationary wind model.

(2) The separation of the time-varying trend takes away the additional fluctuating wind, so the nonstationary turbulence intensity is totally smaller than stationary ones. In addition, the rapid variation of wind velocity and direction will cause a prominent nonstationary increase of along-wind turbulence, but has little influence on the cross-wind case.

(3) The along-wind and cross-wind turbulence integral scales obtained by nonstationary model are much smaller than those from stationary model. The nonstationarity existing in the wind samples will cause an overestimation of turbulence integral scales by the stationary model.

(4) The extraction of time-varying trend results in the disappearance of low-frequency contents in turbulence, so the turbulent energy distribution presented by the nonstationary PSD manifests a descending in low-frequency regions. That is the main reason why the nonstationary PSD is lower than stationary PSD in low-frequency bands but appears almost the same in high-frequency ranges.

(5) For the stationary PSD, the fitted spectrum can well reflect the energy distribution of measured turbulence. However for the nonstationary PSD, the monotonicity of the benchmark model makes the non-monotonicity of the measured nonstationary PSD undescribed, so the nonstationary fitted spectrum can only well satisfy with the measured spectrum in the initial subrange.

(6) In order to consider the non-monotonicity of the nonstationary PSD, a modulating procedure is proposed to modify the fitted nonstationary spectrum with a frequency-modulating function. After modification, the modified fitted spectrum can be almost identical to the measured spectrum, which can be further used to simulate nonstationary turbulence and conduct nonstationary buffeting analyses.

Acknowledgements

The authors would like to gratefully acknowledge the supports from the National Basic Research Program of China (973 Program) (Grant No. 2015CB060000), the National Science Foundation of China (Grant Nos. 51378111 and 51438002), the Basic Scientific & Research Fund of Southeast University (No. 2242015K42028), the Program for New Century Excellent Talents in University of Ministry of Education of China (Grant No. NCET-13-0128) and the Project Funded by the Priority Academic Program Development of Jiangsu Higher Education Institutions (No. CE02-2-15).

References

Bendat J.S. and Piersol A.G. (2010). *Random data: Analysis and measurement procedures*, 4th Ed., Wiley, Hoboken, NJ.

Busch N.E. and Panofsky, H.A. (1968), "Recent spectra of atmospheric turbulence", *Q. J. Roy. Meteorol. Soc.*, **94**(400), 132-148.

Cao, S.Y., Tamura, Y., Kikuchi, N. *et al.* (2015), "A case study of gust factor of a strong typhoon." *Journal of Wind Engineering & Industrial Aerodynamics*, **138**, 52-60.

Cai, C.S., Albrecht, P. and Bosch, H.R. (1999), "Flutter and buffeting analysis. I: finite-element and RPE solution", *J. Bridge Eng.- ASCE*, **4**(3), 174-180.

Counihan, J. (1975), "Adiabatic atmospheric boundary layers: A review and analysis of data from the period 1880–1972", *Atmos. Environ.*, **9**(10), 871-905.

Chen, X.Z. and Kareem, A. (2002), "Advances in modeling of aerodynamic forces on bridge decks", *J. Eng. Mech. - ASCE*, **128**(11), 1193-1205.

Chen, L. and Letchford, C.W. (2004), "A deterministic-stochastic hybrid model of downbursts and its impact on a cantilevered structure", *Eng. Struct.*, **26**, 619-629.

Chen, J., Hui, M.C.L. and Xu, Y.L. (2007), "A comparative study of stationary and non-stationary wind models using field measurements", *Bound. – Lay. Meteorol.*, **122**, 105-121.

Chen, Z.Q., Han Y., Hua X.G. *et al.* (2009), "Investigation on influence factors of buffeting response of bridges and its aeroelastic model verification for Xiaoguan Bridge", *Eng. Struct.*, **31**, 417-431.

Choi, E.C.C. (1978), "Characteristics of typhoons over the South China Sea", *J. Wind Eng. Ind. Aerod.*, **3**, 353-365.

Flay, R.G.J. and Stevenson, D.C. (1998), "Integral length scales in strong winds below 20 m", *J. Wind Eng. Ind. Aerod.*, **28**, 21-30.

Gimsing, N.J. (1983), *Cable Supported Bridge: Concept and Design*, John Wiley and Sons, New York.

Ishizaki, H. (1983), "Wind profiles, turbulence intensities and gust factors for design in typhoon-prone regions", *J. Wind Eng. Ind. Aerod.*, **13**(1-3), 55-66.

Kaimal, J.C., Wyngaard, J.C., Izumi Y. *et al.* (1972), "Spectral characteristics of surface-layer turbulence", *Q. J. Roy. Meteorol. Soc.*, **98**(417), 563-589.

Kareem, A. (1985), "Wind-induced response analysis of tension leg platforms", *J. Struct. Eng. - ASCE*,

111(1), 37-55.
Li, Q.S., Zhi, L.H. and Hu, F. (2009), "Field monitoring of boundary layer wind characteristics in urban area", *Wind Struct,*, **12**(6), 553-574.
Meng, Y., Matsui, M. and Hibi, K. (1997), "A numerical study of the wind field in a typhoon boundary layer", *J. Wind Eng. Ind. Aerod.*, **67-68**, 437-448.
McCullough, M. and Kareem, A. (2013), "Testing stationarity with wavelet-based surrogates", *J. Eng. Mech. - ASCE*, **139**(2), 200-209.
Ni, Y.Q., Xia, Y., Lin, W. *et al.* (2012), "SHM benchmark for high-rise structures: a reduced-order finite element model and field measurement data", *Smart Struct. Syst.*, **10**(4-5), 411-426.
Ou, J.P. and Li, H. (2010), "Structural health monitoring in mainland of China: review and future trends", *Struct. Health Monit.*, **9**(3), 219-231.
Von Karman, T. (1948), "Progress in the statistical theory of turbulence", *Proceedings of the National Academy of Sciences of the United States of America*, **34**(11), 530-539.
Simiu, E. and Scanlan, R.H. (1978), *Wind effects on structures: an introduction to wind engineering*, John Wiley & Sons, Inc., New York.
Wang, L. and Kareem, A. (2004), "Modeling of nonstationary wind in gust-fronts", *Proceedings of the 9th ASCE Joint Specialty Conference on Probabilistic Mechanics and Structural Reliability*, New Mexico.
Wang, H., Li, A.Q., Niu, J. *et al.* (2013), "Long-term monitoring of wind characteristics at Sutong Bridge site", *J. Wind Eng. Ind. Aerod.*, **115**, 39-47.
Wu, T. and Kareem, A. (2015), "A nonlinear analysis framework for bluff-body aerodynamics: A Volterra representation of the solution of Navier-Stokes equations", *J. Fluids Struct.*, **54**, 479-502.
Wu, T. (2015), "Simulation of nonstationary wind velocity field utilizing multi-scale spatial correlation nested Hilbert-Wavelet scheme", *Proceedings of the 14th International Conference on Wind Engineering* (ICWE14), Porto Alegre, Brazil.
Xu, Y.L., Zhu, L.D., Wong K.Y. *et al*. (2000), "Field measurement results of Tsing Ma suspension Bridge during Typhoon Victor", *Struct. Eng. Mech.*, **10**(6), 545-559.
Xu, Y.L. and Chen, J. (2004), "Characterizing nonstationary wind speed using empirical mode decomposition", *J. Struct. Eng.- ASCE*, **130**(6), 912-920.
Ye, X.W., Ni, Y.Q., Wai, T.T. *et al*. (2013), "A vision-based system for dynamic displacement measurement of long-span bridges: algorithm and verification", *Smart Struct. Syst.*, **12**(3-4), 363-379.
Yu, B., Chowdhury, A.G. and Masters, F.J. (2008), "Hurricane wind power spectra, cospectra, and integral length scales", *Bound. –Lay. Meteorol.*, **129**, 411-430.
Zhu, L.D. and Xu, Y.L. (2005), "Buffeting response of long-span cable-supported bridges under skew winds. Part 1: theory", *J. Sound Vib.*, **281**, 647-673.